International Journal of Research and Review
Vol. 9; Issue: 1; January 2022
Website: www.ijrrjournal.com
Review Article *E-ISSN: 2349-9788; P-ISSN: 2454-2237*

Recent Advances in Doped Bi_2O_3 and its Photocatalytic Activity: A Review

Bella Aprimanti Utami[1], Heri Sutanto[1,3], Eko Hidayanto[1], Ilham Alkian[2,3]

[1]Department of Physics, Faculty of Science and Mathematics, Diponegoro University, Semarang-Indonesia
[2]Department of Environmental Science, Graduate School, Diponegoro University, Semarang-Indonesia
[3]Smart Materials Research Center (SMARC), Diponegoro University, Semarang-Indonesia

Corresponding Author: Heri Sutanto

DOI: https://doi.org/10.52403/ijrr.20220128

ABSTRACT

Bismuth Oxide (Bi_2O_3) has a very promising photocatalytic ability to degrade waste pollutants under visible light irradiation because it has a small energy gap of around 2.85-2.58 eV. Although it has excellent potential as a photocatalyst, Bi_2O_3 has the disadvantage of a high electron-hole pair recombination rate, which will reduce its photocatalytic activity. To overcome these problems, surface modifications, defect recognition, or doping of Bi_2O_3 are carried out to obtain a more effective and efficient photocatalyst to degrade waste pollutants under visible light irradiation. Several studies by researchers have been described for the modification of Bi_2O_3 by doping. Various types of doping are given, such as doping in elements or doping in the form of compounds to form composites. Based on several studies that have been described, appropriate doping has been shown to increase the photocatalytic activity of Bi_2O_3.

Keywords: Bi_2O_3, Photocatalyst, Doping

INTRODUCTION

The growth of the modern industry is getting faster in recent years has led to an increase in environmental pollution, especially water pollution. Pollution of the water environment is a severe problem and must be solved because the water environment is one of the sources of life for living things. If the water environment is polluted, it will threaten the ecosystem and the health of living things[1]. Water pollution from industrial and medical waste is a source of considerable pollution in water environmental problems if the waste is discharged directly into the river without any special treatment. The waste's toxic, accumulating, and potentially carcinogenic nature poses a severe threat to the aquatic environment. Therefore, an effective and efficient method is needed to overcome this water pollution problem[2-4]

Advanced Oxidation Process (AOPs) has been widely used as an environmentally friendly, green process method, and cost-effective so that it is more productive in providing solutions to water environmental problems. AOPs involve the generation of hydroxyl radicals in sufficient quantities to affect water purification and utilize the oxidation reaction process[5]. Photocatalytic technology shows good prospects for use in this technique because it can carry out oxidation reactions and generate hydroxyl radicals and be sustainable and environmentally friendly[6].

Semiconductor photocatalysts have been widely applied to overcome the problem of water pollution. Several semiconductors such as TiO_2, ZnS, and ZnO have been widely applied to degrade pollutants in the aquatic environment under Ultra Violet (UV) light irradiation. However, due to the amount of UV light from solar radiation is less than visible light, it is crucial to take advantage a widely used of visible light. So it is necessary to do

further research for other photocatalysts that are more efficient and able to work in visible light[7]. As an attractive photocatalytic material, Bismuth oxide (Bi_2O_3) has been widely studied for its easy synthesis, controllable energy gap, and high visible light response[8-9].

Bi_2O_3 is a p-type metal oxide semiconductor with a narrow energy gap of 2.85-2.58 eV, which can be widely used as a photocatalyst in visible light[9]. The characteristics of Bi_2O_3 are auspicious for application as a photocatalyst such as high redox reversibility, significant photoluminescence, refractive index, photoconductivity, and dielectric permittivity, as well as low resistivity[10]. There are five crystallographic polymorphs of Bi_2O_3, namely (monoclinic), (tetragonal), (cubic bcc), (cubic fcc), and (orthorhombic)[11]. The phase change cycle of Bi_2O_3 can be seen in [Fig 1].

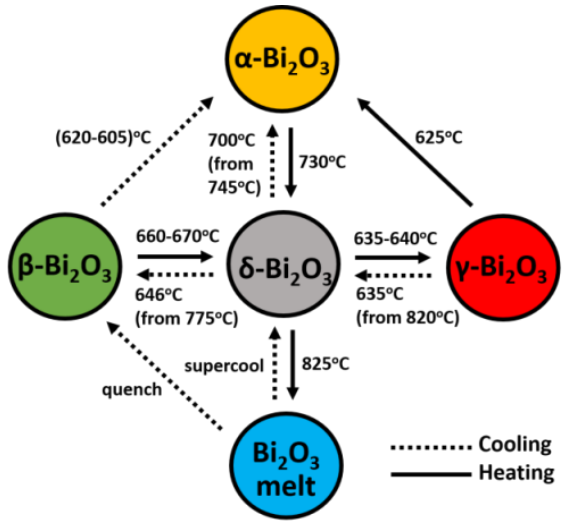

Fig 1: Bi_2O_3 phase transformation

Increasing the temperature in the α-Bi_2O_3 phase°C to 730°C obtained the δ-Bi_2O_3 phase, which is stable to the melting point at 824°C, cooling the δ-Bi_2O_3 phase at 646°C produces the β-Bi_2O_3 phase or γ-Bi_2O_3 phase at 639°C. The β-Bi_2O_3 phase changed to the α-Bi_2O_3 phase on cooling to 303°C, and the γ-Bi_2O_3 phase at 500°C. The transition to the γ-Bi_2O_3 phase can also occur by cooling δ-Bi_2O_3 at 635-640°C. The α-monoclinic and γ-cubic bcc phases are semiconductors, while the β-tetragonal and γ-cubic fcc are excellent conductors of oxide ions and can be considered anion-deficient fluorite structures bismuth occupies the fcc site, undergoing oxygen sublattice defects. The γ-Bi_2O_3phase can stand up to room temperature with a slow cooling rate. The highest conductivity occurs in the δ-Bi_2O_3 phase[12-13]. There is a stable phase at low temperature, namely α-Bi_2O_3, and a stable phase at high temperature, namely δ-Bi_2O_3; the other three are metastable phases[14].

Some of the characteristics of Bi_2O_3 described have the potential to make it a photocatalyst. However, using pure Bi_2O_3 as a photocatalyst has some drawbacks, such as relatively low photocatalytic activity and a high electron-hole pair recombination rate. To overcome this problem, it is necessary to modify the surface, identify defects, or doping Bi_2O_3 to obtain a more effective and efficient photocatalyst to degrade waste pollutants under visible light irradiation. Several researchers have modified Bi_2O_3 by doping. The types of doping given vary, such as doping elements and compounds to form composites. Several studies will be discussed in this journal for the doped and synthesized Bi_2O_3 photocatalyst using the precipitation method. Precipitation is one method of material synthesis that is relatively easy to do because it does not require complex technology, only mixing reagents with precipitating agents. In addition, it can be carried out at room temperature and produces higher yields[15].

PHOTOCATALYST Bi_2O_3

Sonal, S. and R. Sharma[16], have succeeded in synthesizing α-Bi_2O_3 doping Ni by the precipitation method. The X-Ray Diffraction (XRD) pattern obtained has a α-Bi_2O_3 phase based on JCPDS: 00-041-1449, which indicates no crystal structure deformation or phase change due to Ni doping. However, the existence of Ni doping causes the peak intensity decreased slightly, indicating a reduction in the crystallinity of the doped sample. The Ni-doped α-Bi_2O_3 sample experienced a slight

shift in the value of 2θ towards the right to become more comprehensive. The Ni-doped α-Bi_2O_3 Scanning Electron Microscope (SEM) image shows a rod-like morphology with non-uniform or broken dimensions with an average 15–22 μm. The addition of Ni causes morphological changes in α-Bi_2O_3 provide a rougher surface area due the structure forms broken and irregular rods to help the photoreaction process be better. The α-Bi_2O_3/Ni energy gap is lower than that of pure α-Bi_2O_3, which is 2.58 eV. The photocatalytic activity of Ni-doped α-Bi_2O_3 samples was carried out by analyzing the photodegradation of Methylene Blue (MB), and showed an increase compared to pure α-Bi_2O_3. The color change ratio was up to 50% throughout 275 minutes before doping. After doping, there was an increase in the ratio, almost 81% MB degraded over the same time duration.

In addition, Meng, Q and Z. Ying[17], have also succeeded in synthesizing Bi_2O_3/Ni with a Ni concentration of 1-5% (%mol) using the precipitation method. However, in this study, the addition of Ni caused a change in the crystalline phase of Bi_2O_3. XRD pure Bi_2O_3 diffraction pattern indicated as monoclinic α-Bi_2O_3 phase based on JCPDS: 71-0465. The addition of Ni 1% to Bi_2O_3 causes the peaks of α-Bi_2O_3 to disappear gradually, but several new prominent peaks appear and are confirmed as tetragonal β-Bi_2O_3 phase according to JCPDS: 49-1762. When the Bi/Ni molar ratio is 2%, sample of α-Bi_2O_3 completely changes to tetragonal β-Bi_2O_3. The crystal sizes of the 0-5% Bi_2O_3/Ni are 53.5; 39.1; 35.7; 32.4; 32.8; and 41.8 nm. Doping Ni 3% has the smallest crystal size, its morphology shows a perfect microsphere structure. Increasing the concentration of Ni further displays a flower-like structure. The energy gap of 3% Bi_2O_3/Ni is 2.37 eV, and pure Bi_2O_3 is 3.06 eV. The photocatalytic activity was performed by degrading pyridine under visible light radiation for 60 minutes. The result was that the Bi_2O_3/Ni photocatalyst was much higher in performance than Bi_2O_3. The best performance was observed in 3% Bi_2O_3/Ni with a degradation efficiency of around 93%.

Malathy, P and colleagues[18], have succeeded in synthesizing Bi_2O_3 doped transition metals (Ni and Zn) by precipitation method. Based on the results, the XRD pattern of the sample showed that the crystal structure of Bi_2O_3 was not affected, but after doping with Ni and Zn the peak intensity changed. All diffraction peaks were formed entirely and indicated as tetragonal β-Bi_2O_3 phase according to JCPDS: 65-1209. Due to transition metals doping, diffraction peaks did not appear due to higher dispersion and their low content. The average crystal sizes of β-Bi_2O_3 was 17 nm, Bi_2O_3/Ni was 23 nm, and Bi_2O_3/Zn was 20 nm. The results of the sample morphology analysis by SEM showed that β-Bi_2O_3, Bi_2O_3/Ni had a stem-like structure and Bi_2O_3/Zn had a flower-like structure. The addition of transition metals causes this morphological change. The presence of Ni ions in Bi_2O_3 shows a significant redshift of the absorption peak towards the visible light region compared to Bi_2O_3 with energy gaps for β-Bi_2O_3, Bi_2O_3/Ni, and Bi_2O_3/Zn are 2.8; 2.69; and 2.74 eV respectively. The narrower energy gap of Bi_2O_3/Ni can have photocatalytic activity in visible light, which is very good than Bi_2O_3/Zn and Bi_2O_3. The degradation of Malachite Green (MG) under visible light irradiation with an irradiation duration of 180 minutes was used to evaluate the photocatalytic activity of Bi_2O_3/Ni. The results show that Bi_2O_3/Ni has better photocatalytic activity than other photocatalysts. This corresponds to the energy gap obtained, which is the smallest.

The synthesis of Bi_2O_3/Zn was also carried out by Viruthagiri, G. and colleagues[19], using a simple chemical precipitation method. Diffraction peaks of Bi_2O_3 indicated as monoclinic α-Bi_2O_3 phase according to JCPDS: 71-0465, the phase structure did not change after Zn doping. Pure Bi_2O_3 has a size of 57.2 nm, while after doping 1-5% Zn (%mol) the crystal size decreases to 42.94-54.56 nm.

The pure Bi_2O_3 morphology shows many needle- or rod-shaped structures with sharp edges, whereas Bi_2O_3/Zn shows a well-isolated rod morphology with a porous structure and rough particle surface. The energy gap of pure Bi_2O_3 is 2.65 eV, while the energy gap of 1-5% Bi_2O_3/Zn is around 2.76-2.68 eV. The photocatalytic activity of Bi_2O_3/Zn was investigated based on the degradation of Methylene Blue dye solution under visible light irradiation. The results showed that after 135 minutes of irradiation, Bi_2O_3 showed partial degradation of the dye, while the doped samples showed complete degradation. Bi_2O_3/Zn showed a 95% higher degradation efficiency than pure Bi_2O_3.

In addition to Ni and Zn doping, Viruthagiri G and P. Kannan[20], conducted a study to synthesize cobalt (Co) doped Bi_2O_3 using the precipitation method. Doping was carried out with different Co concentrations (0.05-0.25 M). The XRD pattern of pure Bi_2O_3 nanoparticles was confirmed to have a monoclinic α-Bi_2O_3 crystal structure (JCPDS No. 71-0465). There are no peaks associated with cobalt or cobalt oxide in the Bi_2O_3 phase. However, the doping effect causes a non-monotonic shift in the diffraction pattern towards a wider 2θ region. The crystal size and lattice parameter values decrease gradually with Co doping. The surface morphology of pure Bi_2O_3 and Bi_2O_3/Co (0.15 M) analyzed by Field Emission-Scanning Electron Microscope (FE-SEM) showed that Bi_2O_3 has a morphology like nanosheets, while Bi_2O_3/Co (0.15 M) consists of many narrow nanoplates that are interconnected. Based on the UV-Vis Bi_2O_3/Co spectrum, as the concentration of Co doping increases, the absorption edge shifts towards a wider wavelength region, indicating a decrease in the energy gap of Bi_2O_3. The energy gap of Bi_2O_3/Co (0.05-0.25 M) decreases with increasing dopant concentration from 2.21 eV to 1.94 eV, while pure Bi_2O_3 is 2.64 eV. The photodegradation of Methylene Blue dye solution under visible light irradiation for 135 min was carried out to evaluate the photocatalytic activity of Bi_2O_3 and Bi_2O_3/Co (0.15 M), and showed the best catalytic activity with a degradation efficiency of 97%, while pure Bi_2O_3 was only 76.15%.

Synthesis to produce a silver-doped Bi_2O_3 photocatalyst with a Bi/Ag molar ratio of 1-9% (%mol) by co-precipitation method was carried out by Li, Y and colleagues[21]. The XRD pattern shows that the composition of all samples is monoclinic α-Bi_2O_3 phase (JCPDS: 41-1449). In addition, the typical face-centered cubic (fcc) structure of Ag metal (JCPDS: 04-0783) was indicated in the formation of pure silver with low crystallinity observed in the 9% Bi_2O_3/Ag XRD pattern. The Transmission Electron Microscope (TEM) analysis showed that the sample consisted mainly of high crystallinity nanosheets. Bi_2O_3/Ag nanosheets show high absorption in the visible light region. The energy gap of Bi_2O_3/Ag (2.59-2.25 eV) is lower than that of pure Bi_2O_3 (2.63 eV). The photocatalytic activity tested by degrading Methyl Orange (MO) under visible light irradiation. With duration off irradiation for 180 minutes, Ag 3% doped on Bi_2O_3 had the most optimal photocatalytic activity. The experimental results show that the rate of photocatalytic activity of Bi_2O_3/Ag is 3.45 times compared to pure Bi_2O_3. The photocatalytic activity Bi_2O_3/Ag had better than pure Bi_2O_3, attributed to the Ag-doped nanosheet structure offering high electron-hole pair separation. Doping Ag was able to increase Bi_2O_3 activity, but excessive Ag doping causes a problem in the heterojunction structure acts as a charge carrier recombination center for electron and hole pairs. Defects and oxygen vacancies of the Bi_2O_3 lattice due to excessive Ag doping affect the decrease in photocatalytic activity of Bi_2O_3/Ag samples (5-9%).

Liang, J and colleagues[22], have synthesized Bi_2O_3/Fe porous microspheres. The results of the XRD pattern analysis showed that the crystal formed was a tetragonal β-Bi_2O_3 phase (JCPDS: 65-1209). Fe^{3+} ions undergo substitution to Bi^{3+} ions

in the Bi_2O_3 lattice structure but are not affected in the Bi_2O_3 crystal lattice. The SEM image shows that pure β-Bi_2O_3 has a porous microsphere structure with a diameter of about 7 μm. The microsphere structure consists of many Fe nanoparticles. UV-Vis spectra showed that Bi_2O_3/Fe had strong visible light absorbance in the wavelength range from 420 nm to 600 nm. The energy gap ranges from 2.25-1.67 eV. Increased absorption of visible light and decreased energy gap can increase the photocatalytic activity of β-Bi_2O_3. Photodegradation of Methyl Orange was tasted to determine the photocatalytic activity of Bi_2O_3/Fe. It was observed that the Methyl Orange dye molecule was able to degrade better using a Bi_2O_3/Fe photocatalyst than pure β-Bi_2O_3under visible light irradiation with an irradiation duration of 60 minutes, the degradation rate of 0.0328 min^{-1} was obtained.

Sudrajat, H. et. al.[23], has conducted a study by applying two strategies simultaneously to improve Bi_2O_3 photocatalytic properties. The first strategy through carbon (C) and nitrogen (N) doping is simultaneously able to increase the absorption of visible light region, and the second strategy is Fe(III) grafting to increase the charge carrier separation. The synthesis results showed that Bi_2O_3 have diffraction peaks according to cubic δ-Bi_2O_3 phase based on JCPDS: 52-1007. There did not indication of crystal phase and other impurities after C-N doping without Fe(III) grafting, but the intensity of diffraction peaks decreased and widened slightly, this may occur due to urea which inhibition of crystal growth during calcination. The crystal phase did not change after Fe (III) grafting, and the peak intensity were relatively similar. The existence of Fe (III) was only on the surface of Bi_2O_3 so that it did not change the microstructural of Bi_2O_3. Surface morphology analyzed using SEM showed that 0.2% Fe(III)-C/N-Bi_2O_3 have average diameter of 130 nm in the form of nanospheres. The absorption edge of Bi_2O_3 is around 475 nm with an energy gap of 2.61 eV. The Fe (III) grafting process and C/N doping did not change the Bi_2O_3 gap energy value. However, as a result of C/N doping and Fe(III) grafting displayed two peaks absorption in the visible light region So, C/N doping and Fe(III) grafting in principle can increase light absorption without changing the energy gap. The Fe(III)-C/N-Bi_2O_3 0.2% photocatalyst had a degradation efficiency of 87% and showed excellent photocatalytic performance for decomposing 2.4-dichlorophenol under visible light with an irradiation duration of 60 minutes compared to pure Bi_2O_3 (24%).

The synthesis of Ce^{3+} doped on Bi_2O_3 was carried out by Zhang, W. and colleagues[24]. XRD confirmed the crystallinity properties of the resulting material. Diffraction peaks of commercial nanoparticles Bi_2O_3 (CNB), hollow needle-shaped Bi_2O_3 (HNB), and HNB-Ce-5 (5% CeO_2 doping) identified were almost the same. Based on the resulting diffraction pattern, CNB and HNB were indicated as monoclinic α-Bi_2O_3 phases (JCPDS: 41-1449)[25]. The peaks diffraction of CeO_2 doped on HNB (HNB-Ce), has the same pattern as pure Bi_2O_3. The phase structure of Bi_2O_3 did not change by dopant CeO_2 due to the small amount of dopant applied on Bi_2O_3 or some CeO_2 can enter the Bi_2O_3 lattice for similar ionic radii[26]. The morphology of CNB an average size of 150 nm. HNB-Ce-5 had hollow needle-shape morphology where the size and surface were larger and rougher than CNB and HNB due to the presence of CeO_2 doping on HNB. The absorption spectrum of CNB has a strong absorption in the UV region. In contrast to CNBs, HNBs exhibit stronger light absorption in the visible light region due to their unique structure. However, HNB-Ce showed a higher light absorption property in the UV and visible light regions (200-800 nm). This suggests that a redshift from the absorption edge to a broader region can be attributed to CeO_2 doping[27]. The energy gap of HNB-Ce is lower than that of CNB and HNB, it indicates that CeO_2 doping can reduce the energy gap of Bi_2O_3

and thereby increase absorption and utilization for visible light. The photocatalytic activity of the sample was evaluated by photodegradation of Tetracycline in a photochemical reactor and a lamp as a visible light source with an irradiation duration of 180 minutes. All HNB-Ce showed better photocatalytic properties than CNB and HNB. HNB-Ce-5 showed optimal photocatalytic properties. The degradation efficiency HNB-Ce-5 reached 89.1%, higher than CNB, HNB, HNB-Ce-3, and HNB-Ce-7 only reached 37.0%; 71.4%; 78.8%; and (76.9%), respectively.

Nagarajan, R. and colleagues[28] have stabilized β-Bi_2O_3 by doping 10% (%mol) thorium with solution combustion synthesis and co-precipitation methods. Diffraction peaks of the samples synthesized by the combustion method was indicated as monoclinic α-Bi_2O_3 phase (ICDD: 76-1730) for undoped samples. The monoclinic symmetry changes to tetragonal when the XRD pattern reveals that 10% Th^{4+} is doped on Bi^{3+} (ICDD: 78-1793). SEM image of sample β-Bi_2O_3 synthesized by the solution combustion method has a peeling-like morphology, while β-Bi_2O_3 synthesized by co-precipitation method shows a porous morphology with an average porous particle diameter of 1.7 nm. β-Bi_2O_3 which is synthesized by the co-precipitation method showed better efficiency due to a decrease in the energy gap. With 10% Th^{4+} in the Bi_2O_3 lattice using the combustion synthesis method, the energy gap decreases from 2.67 eV to 2.24 eV. However, synthesized by the co-precipitation method, the sample of 10% Th^{4+} doped on β-Bi_2O_3 has a drastic decrease of energy gap to 2.02 eV. Photodegradation activity was carried out on Methylene Blue and Rhodamine B under visible light irradiation. Samples are synthesized by the combustion method degrading up to 96% dye with a duration of irradiation for 120 minutes, while the samples are synthesized by the co-precipitation method only takes 90 minutes to degrading with the same percentage degraded. The existence of carbon doping on Bi/Th^{4+}, which is synthesized by the co-precipitation method allows defects in the samples. This is a factor for increasing degradation efficiency in the samples.

Zhang, H. and colleagues[29], synthesized Bi_2O_3/CuNiFe Layered Double Hydroxide (LDHs) composites in the present study. Pure Bi_2O_3 XRD pattern matched with JCPDS: 1-071-2274 and the XRD pattern of CuNiFe LDHs based on JCPDS: 40-0215. Bi_2O_3/CuNiFe LDHs composites indicate all characteristic peaks as Bi_2O_3 peaks and do not shift. There are two peaks of diffraction of CuNiFe LDHs observed on the XRD spectrum for Bi_2O_3/CuNiFe LDHs composite. Morphology of CuNiFe LDHs like flower and layered, spherical Bi_2O_3, agglomerated nanoparticles due to the high surface energy of the Bi_2O_3 particles. The successfully synthesis of the Bi_2O_3/CuNiFe LDHs composite was confirmed with there are many small nanoparticles scattered on the surface of the multi-layered CuNiFe LDHs. Such structures have the potential to increase photocatalytic activity of Bi_2O_3/CuNiFe LDHs composite. The absorption edge of Bi_2O_3 which was evaluated using UV-Vis spectrum is about 465 nm which corresponds to the intrinsic energy gap of Bi_2O_3 (2.82 eV). After combining, the composite LDH Bi_2O_3/CuNiFe showed stronger visible light absorption than LDH $Bi_2O_3$and pure CuNiFe, which indicates that the composite LDH Bi_2O_3/CuNiFe has higher activity for pollutant degradation. It was proven that in sunlight, the degradation efficiency of Lomefloxacin by Bi_2O_3/CuNiFe LDHs was around 84.6% in 40 minutes of irradiation. Pure Bi_2O_3 and CuNiFe LDHs could only degrade 43.2% and 30.4%, respectively.

Wei, Z. et. al.[30], has succeeded in inserting BiOI nanosheets on the porous surface of Bi_2O_3, and it is evenly distributed. The XRD pattern is indicated as a tetragonal BiOI phase (JCPDS: 10-0445) and a monoclinic α-Bi_2O_3 (JCPDS: 41-1449). BiOI doping in Bi_2O_3 produced

diffraction peaks similar to pure BiOI peaks. It cannot be ascertained clearly the peaks diffraction of Bi_2O_3, this is due to Bi_2O_3 being tightly encapsulated by BiOI. In addition, the prominent diffraction peaks of Bi_2O_3 and pure BiOI are very close, so overlapping each other can widen and weaken the XRD BiOI peaks. The characteristic peaks of Bi_2O_3/BiOI are wider than those of pure Bi_2O_3 and BiOI. BiOI's morphology has a diameter of about 1.0-1.5 μm and shows a form like a flower microsphere, and has a thickness of about 10-15 nm shaped nanosheet and see on the edge of the BiOI microsphere. The Bi_2O_3 sample showed 1D porous nanorod morphology with a 300-350 nm diameter. Meanwhile, the 50% Bi_2O_3/BiOI composite maintains a 1D nano rod-like structure with a 500-600 nm diameter. The Bi_2O_3/BiOI composite shows strong light absorption in the visible light region than pure Bi_2O_3. The heterojunction structure by combining BiOI and Bi_2O_3 can increase the absorption of the visible light and reduce recombination rate of electron-hole pair that will increase degradation efficiency, other than the heterojunction structure is also able to expand the specific surface that contributes to the visible light absorption process. Significantly increased for Cr(VI) reduction under visible light irradiation compared to pure Bi_2O_3 and BiOI. In particular, a degradation rate of 94.5% can be achieved from 50% Bi_2O_3/BiOI composite with an irradiation duration of 100 minutes, while only 11.8% and 64.4% degradation efficiency by pure Bi_2O_3 and BiOI.

$Cs_3PMo_{12}O_{40}/Bi_2O_3$ ($CsPMo/Bi_2O_3$) composite was synthesized by Wang, Qi and colleagues[31]. The results showed that CsPMo successfully modified Bi_2O_3. The XRD pattern of the $CsPMo/Bi_2O_3$ composite contains three additional peaks with low intensity relative to pure Bi_2O_3 and are indicated as diffraction peaks of CsPMo. Doping CsPMo with a relativelly low concentration of 2.5% on the Bi_2O_3 surface causes the intensity of the CsPMo diffraction peaks that appears in the $CsPMo/Bi_2O_3$ composite. The pure Bi_2O_3 SEM image shows a flat ellipsoid or beams with a smooth surface, while the $CsPMo/Bi_2O_3$ composite has a rough surface. A relatively rougher surface is usually beneficial for photocatalysis because of the more active interfacial adsorption sites[32]. A redshift of the absorption edge after adding CsPMo to Bi_2O_3 indicated an increase in visible light absorption, which was more relative to pure Bi_2O_3. Compared to Bi_2O_3 (2.76 eV), the energy gap of $CsPMo/Bi_2O_3$ is smaller (2.63 eV), which is beneficial for the utilization of visible light. The photocatalytic activity of the samples was evaluated by Phenol degradation. $CsPMo/Bi_2O_3$ showed the highest activity after 300 minutes irradiation under visible light (83.6%), while for Bi_2O_3 the degradation efficiency was around 48.0% and CsPMo only 12.5%.

Yakot, S. M.[33], also carried out the synthesis to form β-$Ni(OH)_2$ doped α-Bi_2O_3 composite materials. Each samples were synthesized by co-precipitation method, then the formation of β-$Ni(OH)_2$ doped α-Bi_2O_3 composite is done by mechanically mixed with different concentration of each samples. The XRD spectra showed that the monoclinic α-Bi_2O_3 phase and the β-$Ni(OH)_2$ hexagonal phase are well formed. Morphology of each samples are rods and sheets with diameters between 0.9 and 1.1 μm. The energy gap of pure α-Bi_2O_3 is 2.87 eV. While β-$Ni(OH)_2$ doped α-Bi_2O_3 composite (6-18 %wt) have an energy gap around 2.86-2.84 eV. β-$Ni(OH)_2$ doped α-Bi_2O_3 which forms a composite resulted the red shift of absorption edge due to the interaction of α-Bi_2O_3 after being mixed with β-$Ni(OH)_2$ is ascribed to the interface interaction between α-Bi_2O_3 and β-$Ni(OH)_2$ particles. Modifying α-Bi_2O_3 by β-$Ni(OH)_2$ was able to make more effective degrading. β-$Ni(OH)_2$ doped α-Bi_2O_3 composite showed degradation efficiency of 99% for Methylene Blue (80 min), 96% for Congo Red (80 min), 91% for Methyl Orange (180 min), and 90% for 4-nitrophenol (300 min) under visible light irradiation.

$CaFe_2O_4$-Bi_2O_3 heterojunction was successfully synthesized using the ultrasonic-assisted chemical co-precipitation method by Syed, A. and colleagues[34]. The position of the diffraction peaks was found to match those of $CaFe_2O_4$ and Bi_2O_3. The XRD pattern of pure Bi_2O_3 matches the structure of Bi_2O_3. The peak of the hematite phase is formed in the XRD pattern of $CaFe_2O_4$, it is due to the placement of Ca cations by replacing Fe cations in the crystal structure [35]. The XRD pattern of $CaFe_2O_4$-Bi_2O_3 showed similarities to both the peaks of $CaFe_2O_4$ and Bi_2O_3 nanoparticles. Morphological analysis using TEM described $CaFe_2O_4$ nanoparticles in nanospheres on the surface of Bi_2O_3 nanosheets and spread evenly without any aggregation. The photon absorption ability of $CaFe_2O_4$-Bi_2O_3 nanocomposite is in the energy gap region of 2.16 eV. The photodegradation efficiency of $CaFe_2O_4$-Bi_2O_3 was evaluated on Methylene Blue dye. A decrease in the concentration of Methylene Blue was observed under visible light irradiation for 180 minutes. The $CaFe_2O_4$-Bi_2O_3 nanocomposite showed an 8 to 16-fold increase in the kinetic rate constant than Bi_2O_3 and $CaFe_2O_4$ for the degradation of Methylene Blue dye. The $CaFe_2O_4$-Bi_2O_3 nanocomposite is magnetically recoverable with high reusable capacity.

The Bi_2O_3/$FeVO_4$ heterojunction semiconductor was prepared by Liu, X. and Y. Kang[36]. XRD pattern of Bi_2O_3 has a monoclinic α-Bi_2O_3 phase (JCPDS: 41-1449) and all diffraction peaks of $FeVO_4$ are confirmed by JCPDS: 38-1372. Meanwhile, diffraction peaks of Bi_2O_3/$FeVO_4$ heterojunction shows the diffraction peaks of both the crystalline phase of Bi_2O_3 and $FeVO_4$ which proves that the Bi_2O_3/$FeVO_4$ heterojunction has been successfully synthesized. A solid and sharp Bi_2O_3 peak indicates a high degree of crystallinity, while a low $FeVO_4$ peak indicates a low degree of crystallinity. The absorption spectrum of the Bi_2O_3/$FeVO_4$ heterojunction is around 500 nm to 700 nm, this indicates that samples are able to beneficial utilization of visible light more effective and efficient. The energy gap of Bi_2O_3/$FeVO_4$ heterojunction is 2.08 eV, Bi_2O_3 is 2.86 eV, and $FeVO_4$ is 2.26 eV. It shows that the Bi_2O_3/$FeVO_4$ heterojunction can easily induce more electrons and holes by visible light. The photocatalytic activity was tested by degrading Malachite Green for 240 minutes under visible light irradiation. Efficiency degradation of the Bi_2O_3/$FeVO_4$ heterojunction was 88.7% higher than pure Bi_2O_3 (67.9%) and $FeVO_4$ (58.7%).

Ramachandran, S. and A. Sivasamy[37], carried out a synthesis to produce ZnO/Bi_2O_3 composites by precipitation and ultrasonication methods. The crystallinity of the resulting ZnO/Bi_2O_3 nanomaterial with a ratio of 3:1 (ZB3) showed the hexagonal wurtzite structure of ZnO (JCPDS: 36-1451)[38]. In addition, the peak pattern in Bi_2O_3 corresponds to the α-Bi_2O_3 phase monoclinic (JCPDS: 6-294) and tetragonal β-Bi_2O_3 phase (JCPDS: 27-50)[39]. The results of FE-SEM analysis confirmed that the Bi_2O_3 surface are rod-shaped with micro-size. The ZnO nanoparticles structures look typical and no agglomeration occurs. Increased contact between the surface of Bi_2O_3 and ZnO due no agglomeration will increases photocatalytic activity. The optical properties of the nanomaterials were analyzed using UV-Vis DRS (Diffuse Reflectance Spectroscopy) and the results show ZB3 can absorbs light in the visible spectrum with an energy gap of 3.12 eV. The composite energy gap is lower than ZnO. The shift of absorption peak due to ZnO modification with Bi_2O_3 can extended its photoactivity. The nano photocatalyst property of ZB3 was explored by conducting experiments on the photocatalytic degradation of Acid Red-85 dye under visible light irradiation. After 240 minutes irradiation, ZB3 degradation efficiency reached 93.53%

Bi_2O_3-bentonite nanocomposite was successfully synthesized by Patil, S. P. and colleagues[40] to degrade Rhodamine B. The

results of XRD analysis showed that all the Bi_2O_3-bentonite diffraction patterns were similar to the Bi_2O_3 diffraction patterns[41], but there are peaks widening on Bi_2O_3-bentonite compared to pure Bi_2O_3. The morphology of the samples analyzed using SEM showed that Bi_2O_3 has the form of nanorods, it is clear that the Bi_2O_3 nanorods are well dispersed on the bentonite. Bentonite, Bi_2O_3, and Bi_2O_3-bentonite are used for degrading of Rhodamine B with a duration of irradiation in visible light for 80 minutes. The percentage of Rhodamine B degradation by bentonite, Bi_2O_3, and Bi_2O_3-bentonite after 80 minutes of adsorption were 62%, 58.4% and 98.5%, respectively. Intercalation between bentonite and Bi_2O_3, increasing light absorption and decreasing electron-hole pair recombination can increase photocatalytic efficiency than pure Bi_2O_3.

Zhu, W, and colleagues[41], synthesized Bi_2O_3/CuO composites using the co-precipitation method. Based on XRD analysis, the CuO diffraction peak was not detected, but what was detected was the $Bi_{7.38}Cu_{0.62}O_{11.69}$ peak (JCPDS: 00–049-1765). A new compound replaced the disappearance of the CuO peak. On the other hand, the main feature of Bi_2O_3 is still maintained, which is confirmed by JCPDS: 03–065-2366. $Bi_{7.38}Cu_{0.62}O_{11.69}$ grows on the surface of Bi_2O_3. The results of SEM analysis of pure Bi_2O_3 have irregular shapes and sizes, the particle size ranging from 40 nm to 200 nm. CuO doped on Bi_2O_3 has a morphology like seedlings (CuO) that grows on the surface of Bi_2O_3 and forms nanoparticles. Pure Bi_2O_3 and Bi_2O_3/CuO composites have a strong absorption capacity for UV light. At a wavelength of 380 nm, the absorption curve of pure Bi_2O_3 decreases sharply, but Bi_2O_3/CuO composites show superiority with higher absorption in the visible light region. The absorption rate of Bi_2O_3/CuO is higher, which is more than three times that of pure Bi_2O_3. The results showed that the addition of CuO extended the absorption range of the photocatalyst from ultraviolet to visible light. The gap energies of Bi_2O_3 and Bi_2O_3/CuO composites are 2.8 eV and 1.9 eV, respectively. The presence of dopants determines the decrease in the energy gap; photon energy utilization is positively affected. Compared with pure Bi_2O_3, Bi_2O_3/CuO nanocomposite showed higher catalytic reaction and photocatalytic efficiency against the target pollutant tetracycline hydrochloride by irradiation by visible light, the obtained degradation efficiency of Bi_2O_3/CuO composite was 97.22%, while the efficiency of pure Bi_2O_3 was 35.12%. After four repeated experimental cycles, the degradation efficiency of Bi_2O_3/CuO composites can still reach more than 90%. This proves that the material has repeated stability for Tetracycline Hydrochloride degradation. These characteristics make Bi_2O_3/CuO composites have practical application value.

Xie, T. and colleagues[42], conducted a study to synthesize $SrFe_{12}O_{19}$ doped β-Bi_2O_3 as a magnetic photocatalyst. Diffraction peaks of $SrFe_{12}O_{19}$ (15%) doped β-Bi_2O_3 were confirmed as β-Bi_2O_3 phase (JCPDS: 27-0050). Diffraction peak from β-Bi_2O_3 on $SrFe_{12}O_{19}$ doped β-Bi_2O_3 was still strong, which indicated that additional of doping did not change phase of β-Bi_2O_3. The result of the XRD pattern analysis confirmed that diffraction peaks of $SrFe_{12}O_{19}$ did not observed due concentration of is low. Morphological analysis of $SrFe_{12}O_{19}$ doped β-Bi_2O_3 was performed using SEM. $SrFe_{12}O_{19}$ has a micron particles structure. Based on JCPDS: 24–1207, $SrFe_{12}O_{19}$ has a hexagonal crystal system and it is proven from the results of SEM analysis that the hexagonal crystals are perfectly formed and the crystal planes grow uniformly. The addition of $SrFe_{12}O_{19}$ had no significant effect, it indicates that composite are well dispersed and heterojunctions structure can be formed which has the potential to make β-Bi_2O_3 more effective in degrading. The results of UV-VIS DRS indicate that absorbance spectrum of $SrFe_{12}O_{19}$ doped β-Bi_2O_3 composite has a strong absorption than β-Bi_2O_3 in visible

light region. The addition of $SrFe_{12}O_{19}$ to β-Bi_2O_3 can decreased of gap energy to 2.38 eV, confirming that $SrFe_{12}O_{19}$ doping could decrease the energy gap and thereby extend the absorbance range. The photocatalytic activity was tested against Rhodamine B using β-Bi_2O_3 and $SrFe_{12}O_{19}$ doped β-Bi_2O_3 composite. The photocatalytic activity increased after doping $SrFe_{12}O_{19}$ 0-15% and the most optimal was obtained at $SrFe_{12}O_{19}$ 15% doping on β-Bi_2O_3 (92.97%) with a visible light irradiation duration of 150 minutes. However, additional 20-25% can decreased photocatalytic efficiency even worse than that of pure β-Bi_2O_3. The degradation rate of pure β-Bi_2O_3 reached 71.32%, while 68.74% for 25% $SrFe_{12}O_{19}$. The gap energy measurement showed that $SrFe_{12}O_{19}$ doped β-Bi_2O_3 composite (25%) has the lowest value. In the theory, the lower gap energy can absorb more visible light but this does not applied, because doping up to 25% causes a decrease of β-Bi_2O_3 content. [Table 1] presents a summary of the photocatalytic activity of the doped Bi_2O_3.

Table 1: Photocatalytic activity of doped Bi_2O_3

Material	Eg (eV)	Pollutant	Duration (Minutes)	Efficiency (%)	Ref
α-Bi_2O_3/Ni	2.58	Methylene Blue	275	81	[16]
β-Bi_2O_3/Ni	2.37	Pyridine	60	93	[17]
β-Bi_2O_3/Ni β-Bi_2O_3/Zn	2.69 2.74	Malachite Green	180		[18]
α-Bi_2O_3/Zn (1-5 %mol)	2.76-2.68	Methylene Blue	135	95	[19]
α-Bi_2O_3/Co (0.05-0.25 M)	2.21-1.94	Methylene Blue	135	97	[20]
α-Bi_2O_3/Ag (1-9 %mol)	2.59-2.25	Methylene Orange	180		[21]
β-Bi_2O_3/Fe (1-5 %wt)	2.25-1.67	Methylene Orange	60		[22]
Fe (III)-C/N-δ-Bi_2O_3	2.61	2.4-dichlorofenol	60	87	[23]
HNB-Ce		Tetracyclin	180	89.1	[24]
β-Bi_2O_3/Th	2.02	MB and RhB	90	96	[28]
Bi_2O_3/CuNiFe LDHs		Lomefloxacin	40	84.6	[29]
Bi_2O_3/BiOI		Cr (VI)	100	94.5	[30]
CsPMo/Bi_2O_3	2.63	Fenol	300	83.6	[31]
α-Bi_2O_3/β-Ni(OH)$_2$ (6-18 %wt)	2.86-2.84	Methylene Blue Congo Red Methyl Orange 4-nirofeniol	80 80 180 300	99 96 91 90	[33]
$CaFe_2O_4$-Bi_2O_3	2.16	Methylene Blue	180		[34]
Bi_2O_3/$FeVO_4$	2.08	Malachite Green	240	88.7	[36]
ZnO/Bi_2O_3 (rasio= 3:1 M)	3.12	Acid Red-85	240	93.53	[37]
Bi_2O_3-bentonit		Rhodamine B	80	98.5	[40]
Bi_2O_3/CuO	1.9	Tetracycline		97.22	[41]
β-Bi_2O_3/$SrFe_{12}O_{19}$	2.38	Rhodamine B	150	92.97	[42]

PHOTOCATALYSIS MECHANISM

Photocatalysts can be defined as materials that can speed up reactions with the help of light energy. The process that occurs in photocatalyst is called photocatalysis. Almost all photocatalyst materials are semiconductor materials because they have an energy gap of about 1-4 eV. The characteristics of an ideal photocatalyst material are that photons can activate it, is chemically unreactive, non-toxic, easy to obtain, and able to utilize a broad spectrum of sunlight[43]. [Fig 2] shows the mechanism of the photocatalytic process.

Pairs of electrons (e^-) and holes (h^+) play a role in determining the reaction process that will take place in both oxidation and reduction states. The photocatalytic process occurs via direct charge transfer consisting of photoinduction carriers or reactive oxygen species (ROS)[44]. Electrons in the valence band will be excited when exposed to sunlight, the process is called the reduction process[45]. Electrons that do not recombine and succeed to the semiconductor surface will adsorb O_2

molecules to form compounds $^{\bullet}O_2^-$ or superoxide anion radicals, reducing species. When a substance molecule meets a hole (h^+), the process is the oxidation process. The hole formed in the valence band will act as an oxidizing agent for H_2O. This hole will react with OH^- which is adsorbed on the surface of the semiconductor to form a hydroxyl radical compound ($^{\bullet}OH$) which is a powerful oxidizing agent and the hole from visible light acts as an oxidizer to become O_2. These reducing and oxidizing species can attack contaminants in water and degrade into harmless compounds[46].

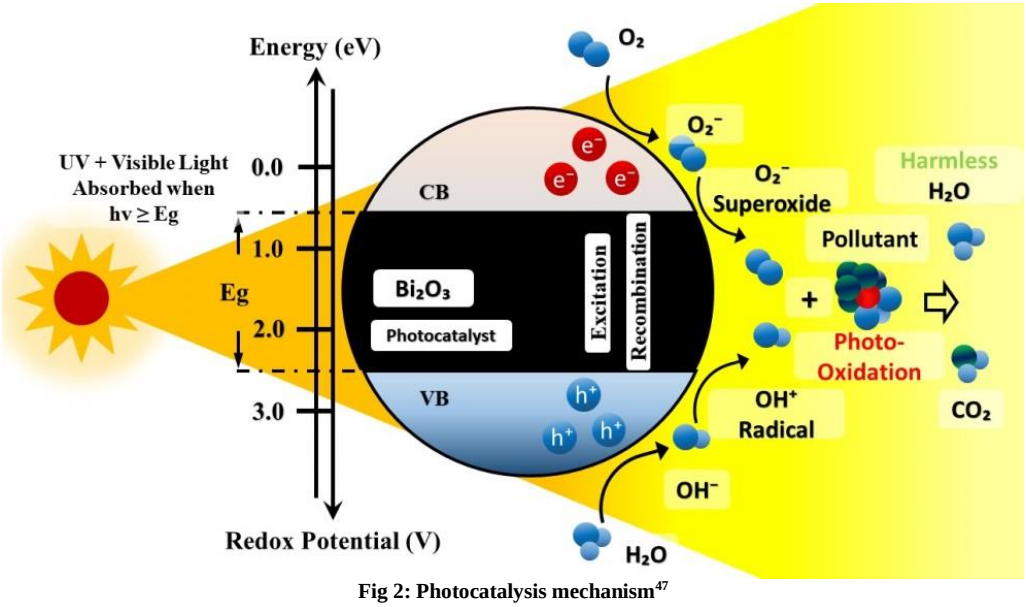

Fig 2: Photocatalysis mechanism[47]

Constraints that often occur in semiconductor photocatalysts are the high rate of electron-hole pair recombination so that the electron lifetime becomes shorter, this affects photocatalytic activity. In the presence of doping, it will be responsible for the electron-hole pair recombination rate and support the increase in photocatalytic activity by suppressing the electron-hole pair recombination rate. However, excessive ion or doping material makes it enter the cluster formation. This cluster can restrain the rate of photodegradation by covering the active site from the surface of Bi_2O_3. Doping material acts as photo-generated between holes and electron transfer, the rate of electron-hole pair recombination during irradiation can be suppressed by increasing the number of trapped electrons to increase the lifetime of electrons and holes. This decrease in the recombination rate increases the photocatalytic activity of Bi_2O_3.

DISCUSSION AND PERSPECTIVE

The dopant Bi_2O_3 photocatalyst increased its photocatalytic activity due to surface modification, widening of the absorption region towards the visible region, and a decrease in the energy gap of the material. The precipitation method carried out the synthesis to produce a powdered material. The use of photocatalysts from granular materials produces residues in the aquatic environment. Therefore, according to the authors, in addition to developing Bi_2O_3 materials that are effective and efficient in degrading, it is also important to consider application techniques that are more environmentally friendly (not causing new problems, such as heavy metal residues).

CONCLUSION

Generally, the photocatalytic activity of semiconductor photocatalysts depends on several factors such as the crystal structure, morphology, surface area, and electronic

structure. Bi_2O_3 photocatalyst doped with elements or compounds to form a composite with precipitation synthesis method can modify pure Bi_2O_3, so that its photocatalytic activity increases. The addition of dopants to Bi_2O_3 with the appropriate concentration will not change the crystalline phase of Bi_2O_3, the surface morphology formed is relatively rougher, and the absorption area is more comprehensive to the visible light region.

Acknowledgement: None

Conflict of Interest: None

Source of Funding: None

REFERENCES

1. Wang X, Yin R, Zeng L, Zhu M. A review of graphene-based nanomaterials for removal of antibiotics from aqueous environments. *Environmental Pollution*. 2019;253:100-110. doi:10.1016/J.ENVPOL.2019.06.067
2. Abdullah H, Susanto Gultom N, Kuo D-H. Indium oxysulfide nanosheet photocatalyst for the hexavalent chromium detoxification and hydrogen evolution reaction. *Journal of Material Science*. 52. doi:10.1007/s10853-017-0858-3
3. Chen X, Zhang W, Luo X, et al. Efficient removal and environmentally benign detoxification of Cr(VI) in aqueous solutions by Zr(IV) cross-linking chitosan magnetic microspheres. *Chemosphere*. 2017;185:991-1000. doi:10.1016/J.CHEMOSPHERE.2017.07.113
4. Li N, Tian Y, Zhao J, et al. Efficient removal of chromium from water by Mn_3O_4@ZnO/Mn_3O_4 composite under simulated sunlight irradiation: Synergy of photocatalytic reduction and adsorption. *Applied Catalysis B: Environmental*. 2017;214:126-136. doi:10.1016/J.APCATB.2017.05.041
5. O'Shea KE, Dionysiou DD. Advanced Oxidation Processes for Water Treatment. *Journal of Physical Chemistry Letters*. 2012;3(15):2112-2113. doi:10.1021/JZ300929X
6. Wang Q, Wang W, Zhong L, Liu D, Cao X, Cui F. Oxygen vacancy-rich 2D/2D BiOCl-g-C_3N_4 ultrathin heterostructure nanosheets for enhanced visible-light-driven photocatalytic activity in environmental remediation. *Applied Catalysis B: Environmental*. 2018;220:290-302. doi:10.1016/J.APCATB.2017.08.049
7. Wang K, Zhang G, Li J, Li Y, Wu X. 0D/2D Z-Scheme Heterojunctions of Bismuth Tantalate Quantum Dots/Ultrathin g-C_3N_4 Nanosheets for Highly Efficient Visible Light Photocatalytic Degradation of Antibiotics. *ACS Applied Materials and Interfaces*. 2017;9(50):43704-43715. doi:10.1021/ACSAMI.7B14275/SUPPL_FILE/AM7B14275_SI_001.PDF
8. Zhang L, Hashimoto Y, Taishi T, Nakamura I, Ni QQ. Fabrication of flower-shaped Bi_2O_3 superstructure by a facile template-free process. *Applied Surface Science*. 2011;257(15):6577-6582. doi:10.1016/J.APSUSC.2011.02.081
9. Xie T, Liu C, Xu L, Yang J, Zhou W. Novel Heterojunction Bi_2O_3/$SrFe_{12}O_{19}$ Magnetic Photocatalyst with Highly Enhanced Photocatalytic Activity. *Journal of Physical Chemistry C*. 2013;117(46):24601-24610. doi:10.1021/JP408627E
10. Matysiak W, Tański T, Jarka P, Nowak M, Kępińska M, Szperlich P. Comparison of optical properties of PAN/TiO_2, PAN/Bi_2O_3, and PAN/SbSI nanofibers. *Optical Materials*. 2018;83:145-151. doi:10.1016/J.OPTMAT.2018.05.055
11. Yilmaz S, Turkoglu O, Ari M, Belenli I. Electrical conductivity of the ionic conductor tetragonal $(Bi_2O_3)_{1-x}(Eu_2O_3)_x$. *Cerâmica*. 2011;57(342):185-192. doi:10.1590/S0366-69132011000200009
12. Shokuhfar A, Nasir K, Esmaeilirad A, et al. Synthesis and characterization of Bismuth oxide nanoparticles via sol-gel method Preparing of Ni-Co/SiO_2 nanocomposite coating by pulse electrodeposition method View project

Thermoelectric Materials View project Synthesis and characterization of Bismuth oxide nanoparticles via sol-gel method. *American Journal of Engineering Researh (AJER)*.. 2014;03:162-165.

13. Deng H-Y, 邓红艳, Hao W-C, 郝维昌, Xu H-Z, 许怀哲. A Transition Phase in the Transformation from α-, β- and ∈- to δ-Bismuth Oxide. *Chinese Physics Letters*. 2011;28(5):056101. doi:10.1088/0256-307X/28/5/056101
14. Lu Y, Zhao Y, Zhao J, et al. Induced aqueous synthesis of metastable β-Bi_2O_3 microcrystals for visible-light photocatalyst study. *Crystal Growth and Design*. 2015;15(3):1031-1042. doi:10.1021/CG500792V/SUPPL_FILE/CG500792V_SI_001.PDF
15. Fatimah, S. HIUAHA. Sintesis Nanokomposit Fe_2O_3/Zeolite buatan sebagai katalis proses Aquathermolisis. *Seminar Kontribusi Fisika 2015*. 2015;3:337.
16. Singh S, Sharma R. Bi_2O_3/Ni- Bi_2O_3 system obtained via Ni-doping for enhanced PEC and photocatalytic activity supported by DFT and experimental study. *Solar Energy Materials and Solar Cells*.. 2018;186(November 2017):208-216. doi:10.1016/j.solmat.2018.06.049
17. Meng Q, Yin Z. Visible light responsive Ni-doped micro/nanostructured Bi_2O_3 microspheres for photocatalytic denitrification of fuel oil. *Mendeleev Communications*. 2019;29(6):672-674. doi:10.1016/j.mencom.2019.11.023
18. Malathy P, Vignesh K, Rajarajan M, Suganthi A. Enhanced photocatalytic performance of transition metal doped Bi_2O_3 nanoparticles under visible light irradiation. *Ceramics International*. 2014;40(1 PART A):101-107. doi:10.1016/j.ceramint.2013.05.109
19. Viruthagiri G, Kannan P, Shanmugam N. Photocatalytic rendition of Zn^{2+}-doped Bi_2O_3 nanoparticles. *Photonics and Nanostructures - Fundamentals Applications*. 2018;32(July 2017):35-41. doi:10.1016/j.photonics.2018.05.008
20. Viruthagiri G, Kannan P. Visible light mediated photocatalytic activity of cobalt doped Bi_2O_3 nanoparticles. *Journal of Materials Research and Technology*. 2019;8(1):127-133. doi:10.1016/j.jmrt.2017.06.011
21. Li Y, Zhang Z, Zhang Y, et al. Preparation of Ag doped Bi_2O_3 nanosheets with highly enhanced visible light photocatalytic performances. *Ceramics International*. 2014;40(8 PART B):13275-13280. doi:10.1016/j.ceramint.2014.05.037
22. Liang J, Zhu G, Liu P, et al. Synthesis and characterization of Fe-doped β- Bi_2O_3 porous microspheres with enhanced visible light photocatalytic activity. *Superlattices and Microstructures*. 2014;72:272-282. doi:10.1016/j.spmi.2014.05.005
23. Sudrajat H, Hartuti S, Park J. A newly constructed photoactive system, Fe(III)-C/N-Bi_2O_3, for efficient visible light photocatalysis. *Journal of Alloys and Compounds*. 2018;748:390-397.
24. Zhang W, Gao S, Chen D. Preparation of Ce^{3+} doped Bi_2O_3 hollow needle-shape with enhanced visible-light photocatalytic activity. *Journal of Rare Earths*. 2019;37(7):726-731. doi:10.1016/j.jre.2018.12.007
25. Shi Y, Luo L, Zhang Y, et al. Synthesis and characterization of porous platelet-shaped α-Bi_2O_3 with enhanced photocatalytic activity for 17α-ethynylestradiol. *Journal of Materials Science 2017 532*. 2017;53(2):1049-1064. doi:10.1007/S10853-017-1553-0
26. Raza W, Haque MM, Muneer M, Harada T, Matsumura M. Synthesis, characterization and photocatalytic performance of visible light induced bismuth oxide nanoparticle. *Journal of Alloys Compounds*. 2015;648:641-650. doi:10.1016/J.JALLCOM.2015.06.245
27. Wang Q, Yu S, Tan Z, et al. Synthesis of monodisperse Bi_2O_3-modified CeO_2 nanospheres with excellent photocatalytic activity under visible light. *CrystEngComm*. 2014;17(3):671-677. doi:10.1039/C4CE02053G
28. Nagarajan R, Pandey J, Kumari P. Thorium doped and thorium-carbon co doped metastable β-Bi_2O_3. *olid State Sciences*. 2019;95(April):105938.

doi:10.1016/j.solidstatesciences.2019.105938

29. Zhang H, Nengzi L chao, Wang Z, Zhang X, Li B, Cheng X. Construction of Bi_2O_3/CuNiFe LDHs composite and its enhanced photocatalytic degradation of lomefloxacin with persulfate under simulated sunlight. *Journal of Hazardous Materials*. 2020;383(May 2019). doi:10.1016/j.jhazmat.2019.121236
30. Wei Z, Zheng N, Dong X, et al. Green and controllable synthesis of one-dimensional Bi_2O_3/BiOI heterojunction for highly efficient visible-light-driven photocatalytic reduction of Cr(VI). *Chemosphere*. 2020;257:127210. doi:10.1016/j.chemosphere.2020.127210
31. Wang Q, Liu E, Zhang C, Huang S, Cong Y, Zhang Y. Synthesis of $Cs_3PMo_{12}O_{40}$/ Bi_2O_3 composite with highly enhanced photocatalytic activity under visible-light irradiation. *Journal of Colloid and Interface Science*. 2018;516:304-311. doi:10.1016/j.jcis.2018.01.065
32. Ma Y, Wu X, Zhang G. Core-shell Ag@Pt nanoparticles supported on sepiolite nanofibers for the catalytic reduction of nitrophenols in water: Enhanced catalytic performance and DFT study. *Applied Catalysis B: Environmental*. 2017;205:262-270. doi:10.1016/J.APCATB.2016.12.025
33. Yakout SM. α-Bi_2O_3/β-Ni(OH)2 composites: Effective solar light photocatalysts for organic pollutants degradation. *Ceramics International*. 2020;46(14):22504-22512. doi:10.1016/j.ceramint.2020.06.010
34. Syed A, Elgorban AM, Bahkali AH, Sillanpää M. Visible-light sensitization and recombination delay through coupling $CaFe_2O_4$ on Bi_2O_3 nanocomposite for high performance photocatalytic and antibacterial applications. *Surfaces and Interfaces*. 2021;26(July). doi:10.1016/j.surfin.2021.101336
35. Zakiyah LB, Saion E, Al-Hada NM, et al. Up-scalable synthesis of size-controlled copper ferrite nanocrystals by thermal treatment method. *Materials Science in Semiconductor Processing*. 2015;40:564-569. doi:10.1016/J.MSSP.2015.07.027
36. Liu X, Kang Y. Synthesis and high visible-light activity of novel Bi_2O_3/ $FeVO_4$ heterojunction photocatalyst. *Materials Letters*. 2016; 164:229-231. doi:10.1016/j.matlet.2015.10.137
37. Ramachandran S, Sivasamy A. Effective charge separation in binary ZnO-Bi_2O_3 photocatalytic material for the treatment of simulated wastewater. *Materials Today: Proceedings*. 2019;17:101-110. doi:10.1016/J.MATPR.2019.06.406
38. Zheng M, Wang ZS, Wu JQ, Wang Q. Synthesis of nitrogen-doped ZnO nanocrystallites with one-dimensional structure and their catalytic activity for ammonium perchlorate decomposition. *Journal of Nanoparticle Research 2009 126*. 2009;12(6):2211-2219. doi:10.1007/S11051-009-9787-7
39. Hou J, Yang C, Wang Z, Zhou W, Jiao S, Zhu H. In situ synthesis of α–β phase heterojunction on Bi_2O_3 nanowires with exceptional visible-light photocatalytic performance. *Applied Catalysis B: Environmental*. 2013;142-143:504-511. doi:10.1016/J.APCATB.2013.05.050
40. Patil SP, Bethi B, Sonawane GH, Shrivastava VS, Sonawane S. Efficient adsorption and photocatalytic degradation of Rhodamine B dye over Bi_2O_3-bentonite nanocomposites: A kinetic study. *Journal of Industrial Engineering Chemistry*. 2016;34:356-363. doi:10.1016/j.jiec.2015.12.002
41. Zhu W, Yu X, Liao J, Fu J, Li Z, Zhang YX. Photocatalytic activity of tetracycline hydrochloride in mariculture wastewater degraded by CuO/Bi_2O_3 under visible light. *Searationp Science Technology (Philadelphia)*. 2021;56(17):2930-2940. doi:10.1080/01496395.2020.1853170
42. Xie T, Yang J, Peng Y, Wang J, Liu S, Xu L. β-Bi_2O_3/$SrFe_{12}O_{19}$ magnetic photocatalyst : facile synthesis and its photocatalytic activity. *Materials Technology*. 2019;00(00):1-8. doi:10.1080/10667857.2019.1638645
43. Banerjee S, Pillai SC, Falaras P, O'shea KE, Byrne JA, Dionysiou DD. New Insights into the Mechanism of Visible Light Photocatalysis. *Journal of Physical*

Chemistry Letters. 2014;5(15):2543-2554. doi:10.1021/JZ501030X

44. Guo MY, Ng AMC, Liu F, Djurišić AB, Chan WK. Photocatalytic activity of metal oxides—The role of holes and OH radicals. *Applied Catalysis B: Environmental*. 2011;107(1-2):150-157. doi:10.1016/J.APCATB.2011.07.008
45. Enzweiler H, Yassue-Cordeiro PH, Schwaab M, Barbosa-Coutinho E, Olsen Scaliante MHN, Fernandes NRC. Evaluation of Pd-TiO_2/ZSM-5 catalysts composition effects on hydrogen production by photocatalytic water splitting. *International Journal of Hydrogen Energy*. 2018;43(13):6515-6525. doi:10.1016/J.IJHYDENE.2018.02.077
46. Syam B, Widyandari H. Sintesis Film Tungsten Oksida (WO_3) dengan Penambahan Metal Co-Katalits dan Besi (Fe) dan Aplikasinya pada Peningkatan Aktivitas Fotokatalitik Degradasi Zat Warna Methylene Blue menggunakan Cahaya Matahari. *Youngster Physics Journal*. 2014;3(1):15-24. doi:10.2/JQUERY.MIN.JS
47. Jalalah M, Faisal M, Bouzid H, Park JG, Al-Sayari SA, Ismail AA. Comparative study on photocatalytic performances of crystalline α- and β- Bi_2O_3 nanoparticles under visible light. *Journal of Industrial and Engineering Chemistry*. 2015;30:183-189. doi:10.1016/J.JIEC.2015.05.020

How to cite this article: Bella Aprimanti Utami, Heri Sutanto, Eko Hidayanto et.al. Recent advances in doped Bi_2O_3 and its photocatalytic activity: a review. *International Journal of Research and Review*. 2022; 9(1): 216-230. DOI: *https://doi.org/10.52403/ijrr.20220128*

******